Direct, Channel-to-Channel Clutter Cancellation (DC4) with Phase-Interferometry in Multi-Channel SAR for Detecting Surface Moving Targets

Dr. P. K. Sanyal, Dr. D. M. Zasada, Mr. R. P. Perry
(psanyal, dmzasada, , rpp)@mitre.org., The MITRE Corp., 26 Electronic Parkway, Rome, NY 13441
Ph: 315-838-2661, Fax: 315-838-2678;

Keywords: Surface Moving Target Indication (SMTI), SAR, Clutter Cancellation, Phase Interferometry.

Abstract

In a Synthetic Aperture Image of the ground, the target motion causes the moving targets to appear at locations different from their true instantaneous locations on the ground. In a corresponding interferometric phase image, all points on the ground nominally appear as a continuum of phase differences while the moving targets appear as discontinuities. By threshold comparisons within the intensity and the phase images, we (and others) have shown that it is possible to detect moving targets in the SAR.

In this paper we show that the detectability of moving targets in multi-channel SAR is further enhanced by a direct, channel-to-channel cancellation of the fixed ground image, which acts as the clutter.

Introduction

In a Synthetic Aperture Image of the ground, the target motion causes the moving targets to appear at locations different from their true instantaneous locations on the ground. In a corresponding interferometric phase image, all points on the ground nominally appear as a continuum of phase differences while the moving targets appear as discontinuities. By threshold comparisons within the intensity and the phase images, we [1, 2, 4, 5] and others have shown that it is possible to detect moving targets in the SAR.

An effect that the motion of the target has is that it causes the moving targets to appear at locations different from their true instantaneous locations on the ground. This is due to the coupling of the cross-range position to the target radial velocity and the fact that the moving target and the ground under it have different radial velocities relative to the platform. The result is the well known phenomenon of 'boat off the wake' or the 'train off the track'.

The Doppler, f_D, of a point at θ radians from the normal to the platform velocity vector V is given by

$$f_D = \frac{2V\sin(\theta)}{\lambda}$$

which, for a small angle θ, reduces to

$$f_D = \frac{2V\theta}{\lambda}$$

If a moving target has the Doppler f_{targ}, then it will appear shifted in cross-range by an angle θ such that

$$f_{targ} = \frac{2V\theta}{\lambda} \; or \; \frac{2v_{targ}}{\lambda} = \frac{2V\theta}{\lambda} \; or \; \theta = \frac{v_{targ}}{V}$$

At a range R, this amounts to a linear shift in cross-range of

$$CrossRangeShift = R\theta = \frac{Rv_{targ}}{V}$$

For R = 22 km, V = 208 m/s and v_{targ} = 30 m/s,

$$CrossRangeShift = \frac{22*10^3*30}{208} = 3.173 \text{ km}$$

Figure 1 shows a 'scene-center stabilized' SAR image of a runway system (X-band data collected by General Dynamics). The figure shows both the Google image of the scene and the SAR image formed from airborne radar collected over this area. The coordinate reference point (CRP) for this image is at the lower left corner of the long runway.

During this collection, there were several GPS-equipped targets moving in a circle near the CRP. There was also a GPS-equipped Cessna propeller-driven aircraft moving on the ground in a separate circle. The left insert in Figure 2 shows these circular paths on the runway.

The 'scene-center stabilized' process makes use of the moving platform's known instantaneous coordinates during a pulse to compute the instantaneous range from the point on the ground and then subtract this range from the range data collected with the pulse. This pre-processing makes the chosen point, referred to as the collection reference point (CRP), to appear at zero Doppler.

Because of the Doppler-to-cross range coupling, objects moving with respect to the underlying ground appear at locations shifted from their actual locations in the SAR image. But it should be recognized that while moving targets appear at shifted locations, they retain the phase value corresponding to their actual location on the ground.

This feature is exploited to detect moving targets via phase interferometry, which is explained in the next section.

The right-insert in Figure 2 shows a close-up of the area of the runway where the targets are operating, overlaid with the computed positions based on GPS data. The target positions are indicated by their assigned numbers. The green numbers indicate the actual positions on the ground while the shifted numbers in red indicate where they appear in the SAR image.

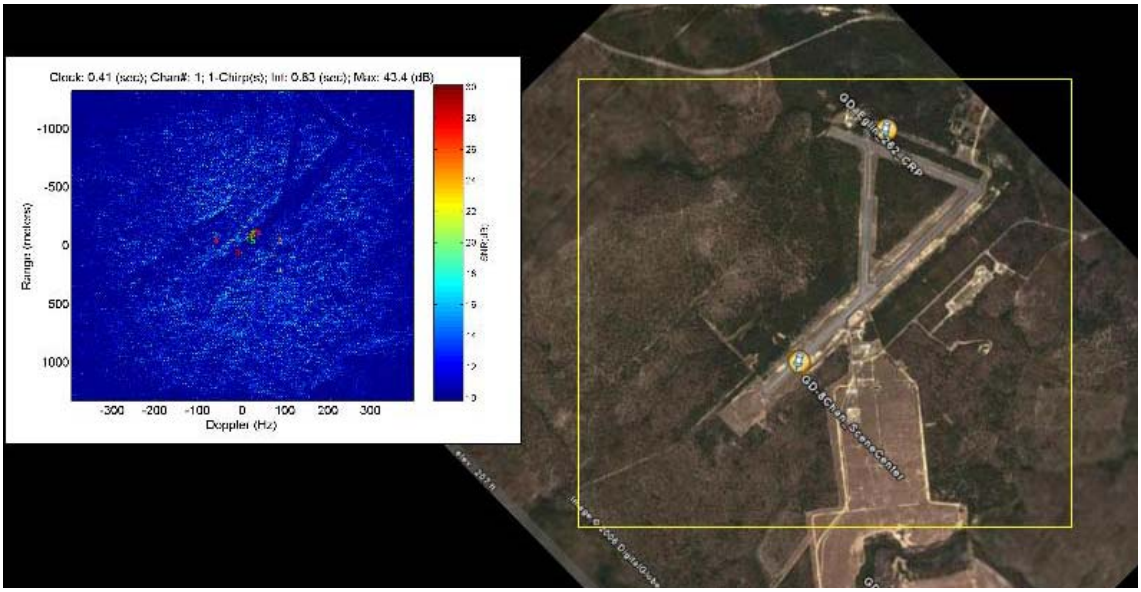

Figure 1. Scene Center Motion-Stabilized SAR Image Eglin Runway Complex (DCS Data)

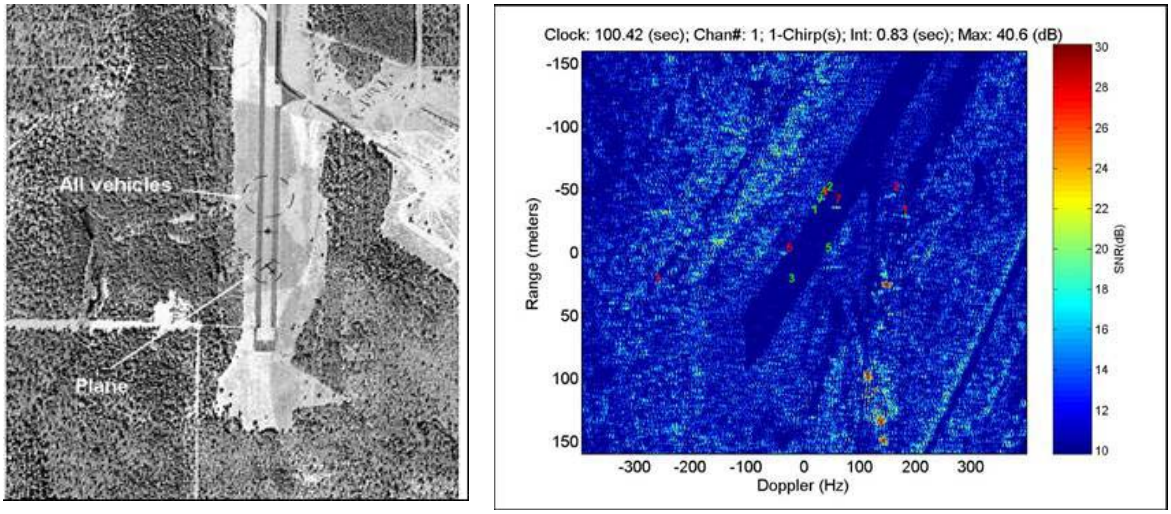

Figure 2. Circling Targets on the Eglin Runway Complex and the RDI Image of the target area

Phase Interferometry Image

The phase-interferometry image is a plot of the phase difference of two SAR images created from any two channels of a multi-channel radar. Figure 3 shows the phase difference image corresponding to the RDI image in Figure 2.

For any two phase-centers (channels) on the radar that are displaced along the velocity vector of the platform, the differences of the phases of the signals received from points on the ground vary (almost) linearly with the cross range and is independent of the strength of the reflected signal. If the phase is color-coded, one would expect to see an image with no other features except a continuously varying color from left to right of the image, with spots of

color anomaly indicating phase anomaly and hence a moving target.

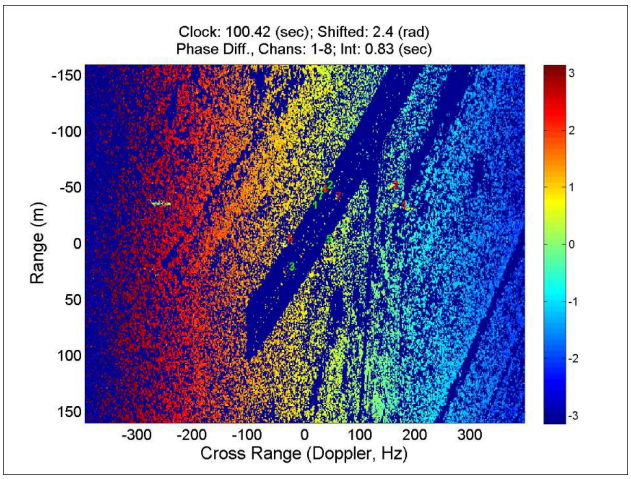

Figure 3. Circling Targets in the Runway Phase Difference Image from channels 1 and 8

In the interferometric phase image, all points on the ground nominally appear as a continuum of phase differences while the moving targets appear as interferometric phase discontinuities because while they appear at displaced locations, they retain their original interferometric phase values that are referenced to their actual location on the ground.

By threshold comparisons within the intensity and the interferometric phase images, we [2, 3, 5] and others [4] have shown that it is possible to detect and geo-locate moving targets in the SAR. An example is shown in Figure 3. In particular, using a QuickSAR technique [2] comparing sequential short-duration, elliptically pixelleted SAR images, we have obtained excellent results detecting moving targets against background scenes and correctly geo-positioning them in composite images.

In Figure 3, one can readily see the phase anomalies associated with the moving targets 1, 2 and 5. The others are not so obvious with the unaided eye but are discernable via automatic detection algorithms.

For automatic detection, we fit a phase plane to the phase difference image and subtract it from the phase difference image. Figure 4 shows the phase values for all the range cells plotted against the Doppler. Ideally, this should have been a single line but clearly the real phase difference deviates significantly from the ideal. The red line is the least-square error fitted plane (edge-view).

This plane is derived as follows. Think of the phase difference image as an mxn matrix of phase difference numbers, where m is the number of range cells and n is the number of Doppler cells, i.e.,

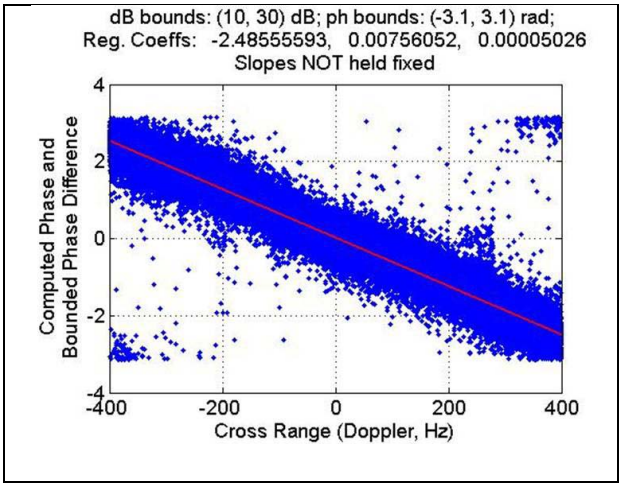

Figure 4. Fitting a plane to the phase difference image

$$\Delta\phi(i,j),$$
$$\text{range cell } i = 1,....,m;$$
$$\text{Doppler cell } j = 1,....,n$$

We intend to fit a plane to this observed surface:

$$\Delta\phi(i,j) = c_0 + c_{range} i + c_{Doppler} j$$

where the c's are the regression coefficients. The phase-difference plane is primarily sloped in the Doppler dimension and therefore $c_{Doppler}$ will have a significant value, but we also allow the plane to be sloped in the range dimension and hence the coefficient c_{range}.

First, create a mxn column vector, $\Delta\bar{\phi}$, of the observed phase differences by first concatenating each row of the phase difference matrix to the previous row and then transposing it:

$$\Delta\bar{\phi} = [\Delta\varphi(1,1), \Delta\phi(1,2), ...\Delta\phi(1,n), \Delta\phi(2,1), \Delta\phi(2,2), ..\Delta\phi(2,n), ..\Delta\phi(m,n)]^T$$

Next, create the (mn)x3 observation matrix, H:

$$H = \begin{bmatrix} 1 & 1 & .....1 \\ 1 & 2 & .....n \quad 1 \quad 2 & .....n \quad 1 \quad 2 & .....n & .....1 \quad 2 & ..n \\ 1 & 1 & 1....1 \quad 2 \quad 2 & .....2 \quad 3 \quad 3 & .....3 \quad ..... & m \quad m & ..m \end{bmatrix}^T$$

We now have the equation

$$\Delta\bar{\phi} = Hc + \upsilon$$
$$\text{where } c \text{ is the regression vector:}$$
$$c = [c_0 \quad c_{Doppler} \quad c_{range}]^T$$
$$\text{and } \upsilon \text{ is the phase noise vector}$$

The well-known [6] weighted least square error estimate of the regression coefficient c is

$$\hat{c} = (H^T R^{-1} H)^{-1} H^T R^{-1} \Delta\bar{\phi}$$

where R is the covariance matrix of the phase noise.

Firstly, we assume that the phase noise in any pixel is independent of the phase noise in any other pixel (though this may not be entirely true since the image is arrived at by a significant amount of processing of the raw data; on the other hand, this may not be a major issue).

Secondly, pixels that have small signal components are dominated by the system noise. Consequently, the phase difference for those pixels will be noisier. Therefore, one is justified in assuming the variance of the noise in any pixel to be inversely proportional to the strength of that pixel. In our computations, we have used a simplified approach to a value to R.

Since the pulse repetition frequency (PRF) of the SAR data is fairly high, the full extent of the SAR image has a large amount of clutter-free space. We can estimate the system noise from this clear area. The image is normalized with respect to this system noise and thus we have the signal to noise ratio (SNR) for each pixel. (In Figure 2, we have excised most of the clear region and displayed only the clutter region in terms of this SNR.).

For computing the regression coefficients for the phase difference plane, we have set a lower threshold for the SNR and simply ignored the pixels that were below this threshold. (We also allowed for an upper threshold to eliminate some extremely strong pixels). When some pixels are ignored, the phase difference vector, $\Delta\bar{\phi}$, is shortened and the corresponding observation matrix, H is modified. For the remaining pixels, we let the R matrix to be an identity matrix.

Having computed the regression coefficients estimates, we compute the 'least square fit' full phase difference vector using the original H matrix:

$$\Delta\hat{\bar{\phi}} = H\hat{c}$$

The mnx1 phase difference vector can now be reshaped back into a mxn matrix. In Figure 4, the red line is the edge view of this fitted plane.

Examining Figure 4 more carefully, one can see that there are phase values at the top right and bottom left corners, which would constitute large phase deviations from the red line. But these are obviously due to the 'fold-over' problem, i.e., they actually belong to the bottom right and top left, respectively, of the plot. After ignoring these, one can discern other phase difference values that deviate significantly from the red line. If we set a threshold of 1 radian, we find that there are still over 40,000 detections, as shown in Figure 5. Clearly, we need to set a magnitude threshold also.

Direct Channel-to-channel Clutter Cancellation (DC4)

Here we report on a technique whereby the stationary ground clutter may be cancelled by using the multiple

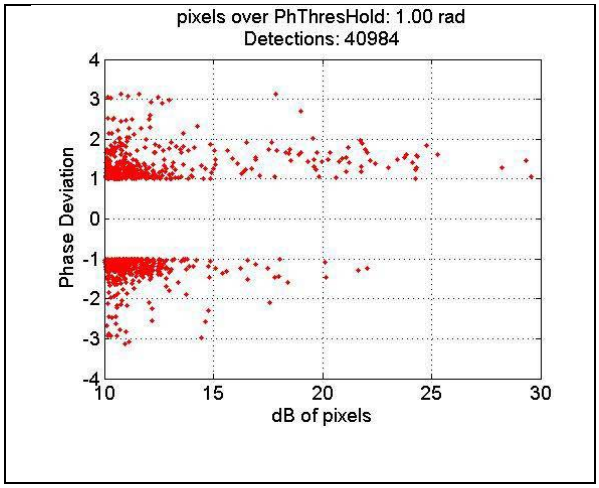

Figure 5. Without clutter-cancellation, more than 40,000 pixels exceed the 1-rad phase difference threshold in the original SAR image

phase centers.

Let the complex images formed at the two channels, numbered 1 and 8, be designated I^1 and I^8 respectively.

Now, ideally (i.e., in the absence of system noise and moving targets) the images I^1 and I^8 are simply phase shifted versions of each other and given the phase shifts, one image can be used to cancel another. To estimate the phase shift, we have performed the least square error fit to the phase difference image. If we now subtract the image from channel 8 modified by this smoothed phase from the channel 1 image, we get the clutter-cancelled image

$$I^{1/8} = I^1 - I^8 \exp(j\Delta\hat{\bar{\phi}})$$

In this clutter-cancelled image, the clutter is cancelled but not the moving target returns because the true phase difference between the target return in the pixel (i, j) is not the same as the smoothed phase difference in pixel (i, j).

Any one channel may be cancelled by any another other channel using the above method. Figure 6 shows some results of enhancing moving target returns by channel-to-channel cancellation of the ground clutter in a channel #2 image using the channel #5 image. The pre-cancellation channel 2 image, not shown here, looks almost identical to the channel 1 pre-cancellation image (the right insert in Figure 2).

To get a measure of the degree of clutter-cancellation that is achieved, we first located the strongest pixel in the pre-cancelled image. After cancellation, we located the same pixel and compared its strength with the previous value. Figure 6 plots these numbers over the 250 image frames from this data set. It appears that on the average, we may expect about 35 dB of cancellation. Considering that we are working with real field-collected data rather than simulated data, this is a fairly high degree of cancellation.

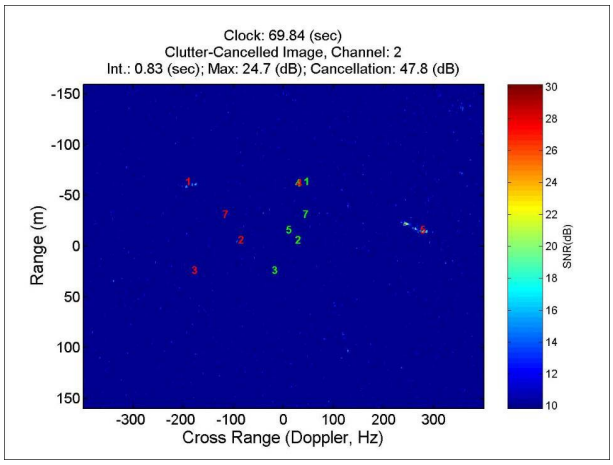

Figure 5. Enhancing Moving Target Returns in SAR Images by Direct Channel-to-Channel Clutter Cancellation

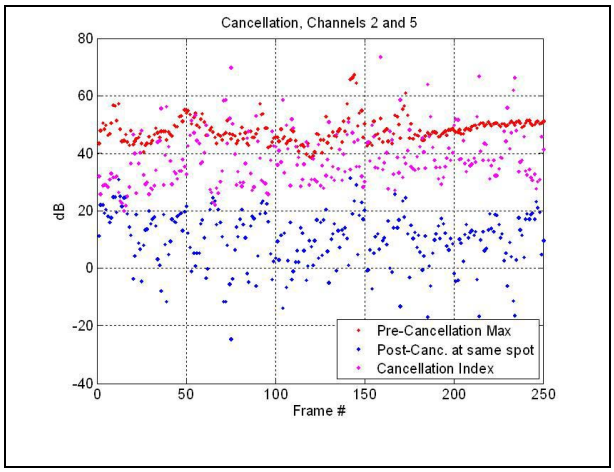

Figure 6. Measured Clutter Cancellation

The Space-Time Adaptive Processing (STAP) [7] technique is the better-known technique for detecting moving targets in clutter and one talks of 'clutter-cancellation' with that technique also. It may be of interest to note that in STAP one does not actually 'subtract' the clutter the way we do here. A brief description of the STAP process is given in the Appendix.

Detecting Moving Target via Double Thresholding

We now search for pixels that exceed a selected magnitude threshold in the clutter-cancelled image and also exceed a selected phase threshold in the reduced phase difference image. We term this 'double thresholding'. The pixels detected as a result of the double thresholding are declared to be moving targets. Figure 7 shows the result of this process.

As in any detection scheme, the realization of a desired probability of detection against a given probability of false alarm is a function of the thresholds selected. Here, we have not yet tried to optimize the thresholds employed, but our preliminary results are encouraging.

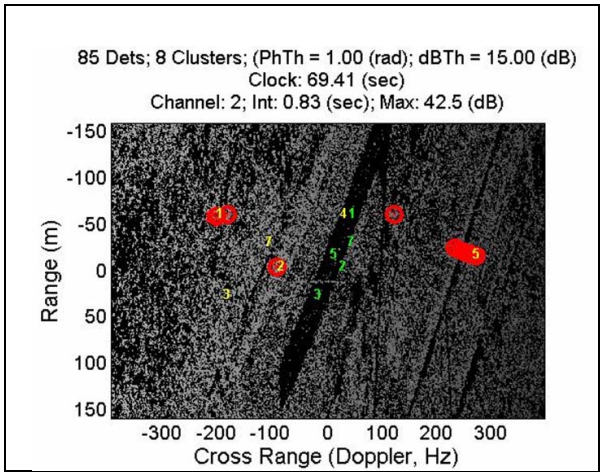

Figure 7. Detecting Moving Targets using Direct Channel-to-Channel Clutter Cancellation and Phase Interferometry

A feature of this particular plot is the absence of excessive false alarms; indeed, there are few in this particular frame. Since the targets are embedded in strong clutter, single threshold processes such as Space Time Adaptive Processing (STAP) often report many false alarms.

CONCLUSIONS

In this paper we have described a novel technique for detecting moving targets in synthetic aperture images (SAR). We have included some results from real data. Our work shows that we can have consistent, automatic detection targets embedded in SAR images where a 'clutter' background must be suppressed to reliably and automatically detect slow moving targets.

References

[1] Sanyal, P. K., Perry, R. P., Zasada, D. M., 'Detecting Moving Targets in SAR Via Keystoning and Phase Interferometry, IRSI-2005, Bangalore, India, December 2005

[2] Sanyal, P. K., Perry, R. P., Zasada, D. M., 'Detecting Moving Targets in SAR via Keystoning and Multiple Phase Center Interferometry', IEEE-2006 Radar Symposium, Verona, NY, April 2006

[3] Stockburger, E. F., Held, D. N., Interferometric Moving Target Imaging, IEEE International Radar Conference, 1995

[4] Zasada, Perry and Sanyal, 'Detecting Moving Targets in Clutter in Airborne SAR via Keystoning and Multiple Phase Center Interferometry', SPIE Defense and Security Symposium 17-21 April 2006 in Orlando, Florida.

[5] Sanyal, P. K., Zasada, D. M., Perry, R. P., 'Tracking Moving Ground Targets from Airborne SAR via Keystoning and Multiple Phase Center Interferometry', IEEE-2007 Radar Symposium, Boston, MA, April 2007
[6] Sage, A. P., 'Optimal Systems Control', Prentice-Hall, Inc., Englewood Cliffs, NJ, 1968
[7] Sanyal, P., 'STAP Processing Monostatic and Bistatic MCARM Data', AFRL-SN-RS-TR-1999-197, Final Technical Report, September 1999

Appendix

Space Time Adaptive Processing (STAP) Algorithms.

There are many versions of STAP algorithms, e.g., Factored Time Space (FTS), Extended Factored Approach (EFA), Joint Domain Localized (JDL), etc. Here we shall very briefly describe the mechanics of the FTS algorithm [7].

For the FTS algorithm, the data is first transformed to the Doppler frequency domain. Now, a frequency-element domain test vector $X_{k,m}$, for range cell k and Doppler m, is formed in this fashion:

$$X_{k,m} = \left[x_{k,m,j}\right]_{j=n}^{j=1}, \qquad n = number\,of\ channels$$

where xk,m,j is the data sample from the kth range cell, mth Doppler bin and jth element or receiver channel. The expanded form of the vector is given below:

$$X_{k,m} = \left[x_{k,m,1}, x_{k,m,2}, x_{k,m,3}, \ldots, x_{k,m,n}\right]^T, \quad n = \#\ of\ channels$$

Next, N_t training data vectors are formed in the same manner as above but from the N_t range cells surrounding the test cell, excluding the desired number of guard cells on either side of the test vector. When possible, half of the N_t cells chosen are below (in range) the test cell and the remaining half above.

The average of the outer-product of these training vectors is the sample covariance matrix for the current range cell k and Doppler bin m, i.e.,

$$\hat{R}_{k,m} = \frac{1}{N_t}\sum_{i=1}^{N_t} X_{i,m} X_{i,m}^H \qquad i \neq k \text{ or the guard cells}$$

The matrix is of dimension nxn where n is the number of channels, and requires that $N_t > 2n$ for a reasonable estimate of the covariance matrix.

The 'adapted' signal value $y_{k,m,l}$ at the test range cell k, test Doppler cell m, and a desired test look angle l is then obtained as:

$$y_{k,m,l} = s_l^{\,H} \hat{R}_{k,m}^{-1} X_{k,m}$$

where s_l is the steering vector corresponding to the look angle l. This is a vector, where n is the number of channels.
Finally, what we usually plot is the normalized value:

$$\bar{y}_{k,m,l} = \frac{(abs(s_l^{\,H} \hat{R}_{k,m}^{-1} X_{k,m}))^2}{s_l^{\,H} \hat{R}_{k,m}^{-1} s_l}$$

Note that unlike the Direct Channel-to-Channel Clutter Cancellation (DC4) method described in the text, the STAP process does not actually 'subtract' any clutter; it 'normalizes'.

The following two plots show the results of applying STAP to a Multi-Channel Airborne Radar Measurement (MCARM) data frame. The L-band MCARM radar had two rows of 11 channels each. And instead of GPS-equipped moving vehicles, an electronic moving target simulator (MTS) was employed. The MTS returned an un-shifted and four Doppler-shifted versions of the impinging waveform.

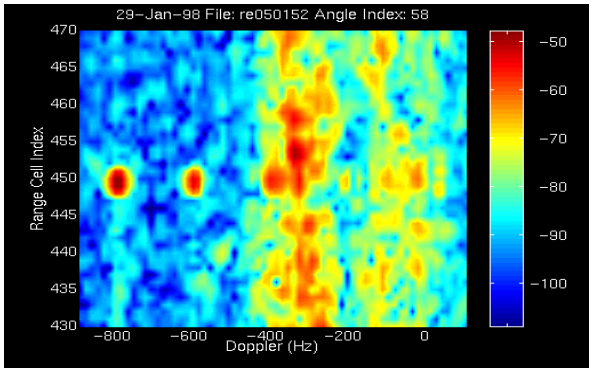

Figure A-1. Un-adapted Image

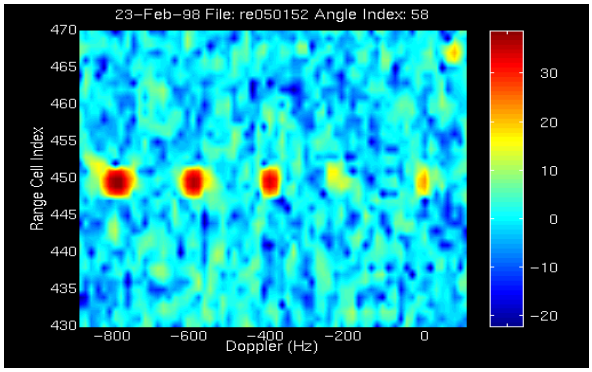

Figure A-2. Adapted Image after Application of the FTS Algorithm

As a part of our continuing work, we plan to compare DC4 and STAP on the same data set, which we have not done so far.